한국지반공학회논문집 제23권 4호 2007년 4월 pp. 185 ~ 197

# Assessment of Tunnel Collapse Load by Closed-Form Analytical Solution and Finite Element Analysis

## 근사적인 해석법과 유한요소해석에 의한 터널붕괴하중 평가

Lee, Yong-Joo[1] 이 용 주


### 요 지

한계해석법인 상·하계법은 점착성, 점착성-마찰성, 마찰성분만 가지는 지반에서의 주로 얕은 터널에 대한 안정수를 구하기 위해 발전되어 왔다. 그러나 점성이 없고 마찰성분만 존재하는 지반에서의 비교적 깊은 터널에 대한 이러한 해석법의 연장은 현재까지 그 연구가 드물게 진행되어왔다. 따라서 본 연구는 이러한 상황에서의 터널붕괴하중을 구하기 위한 근사적인 해석법으로 응력불연속장에 근거하는 하계법과 동적 파괴메카니즘에 근거하는 상계법을 각각 제안하였다. 이러한 해석법에 의한 터널붕괴하중은 수치해석과 기존의 경계해석법과 비교되었으며 특히, 터널 수평축상에 위치하는 유한지반요소들에 대한 유한요소해석 결과와 잘 일치됨을 보여 주었다.

### Abstract

Limit analysis of upper and lower bound solutions has been well developed to provide the stability numbers for shallow tunnels in cohesive soil ($c_u$ material), cohesive-frictional soil ($c' - \phi'$ material) and cohesionless soil ($\phi'$ material). However, an extension of these methods to relatively deep circular tunnels in the cohesionless soil has been explored rarely to date. For this reason, the closed-form analytical solutions including lower bound solution based on the stress discontinuity concept and upper bound solution based on the kinematically admissible failure mechanism were proposed for assessing tunnel collapse load in this study. Consequently, the tunnel collapse load from those solutions was compared with both the finite element analysis and the previous analytical bound solutions and shown to be in good agreement with the FE results, in particular with the FE soil elements located on the horizontal tunnel axis.


**Keywords** : Closed-form analytical solution, Cohesionless soil, Failure mechanism, Finite element analysis, Limit analysis, Stress discontinuity, Tunnel collapse load

## 1. Introduction

The issue of whether undrained or drained conditions are more appropriate to the tunnel stability problem depends principally on the permeability of the soil, the excavation rate, and the size of the tunnel (Mair and Taylor, 1997). As far as upper and lower bound solutions for the tunnel stability in the drained conditions are concerned, relatively few applications are known. In contrast, finite element analysis (FEA) assuming the soil behavior as an elastic-plastic constitutive relationship has been applied to problems in this area to date. The FEA

1 Member, Senior Researcher, Steel Structure Research Laboratory, Research Institute of Industrial Science & Technology (RIST), ucesyjl99@rist.re.kr

* 본 논문에 대한 토의를 원하는 회원은 2007년 10월 31일까지 그 내용을 학회로 보내주시기 바랍니다. 저자의 검토 내용과 함께 논문집에 게재하여 드립니다.

can provide the overall collapse mechanisms associated with the formation of narrow shear bands, although finding tunnel collapse loads for the critical soil elements around the tunnel is a difficult task for the displacement controlled tunnel system rather than for the load controlled tunnel system (Lee, 2004).

Stability of a circular plane strain tunnel for this study can be considered in terms of the idealized geometry shown in Fig. 1. For this study, the relatively deep circular plane strain tunnel ($C/D = 3.7$, $Z_0 = 420$ $mm$) in comparison with the author's shallow model tunnel ($C/D = 2.2$, $Z_0 = 270$ $mm$) without any ground surcharge pressure ($\sigma_s = 0$) was proposed to calculate tunnel collapse load (Lee, 2004).

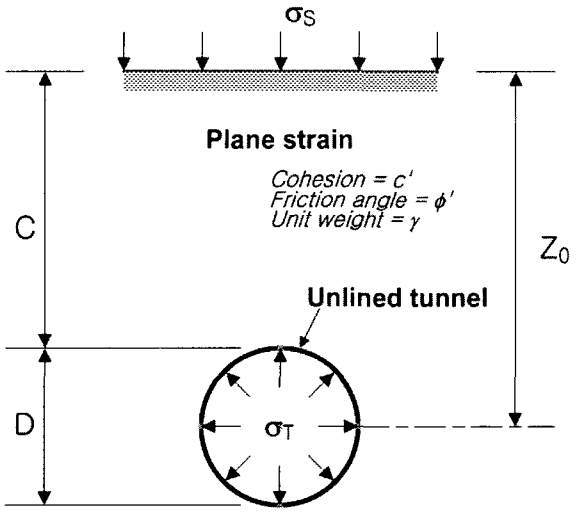


Fig. 1. Geometry of an unlined circular plane strain tunnel (C: tunnel embedded depth from tunnel crown to surface, D: tunnel diameter, $\sigma_S$: surface surcharge load, $\sigma_T$: tunnel internal pressure, $Z_0$: tunnel embedded depth from tunnel centre to surface)

In addition, lower bound solution based on the stress discontinuity concept and upper bound approach based on the kinematically admissible failure mechanisms were proposed and compared with the numerical results by the finite element analysis (FEA) associated with the feed-back data from the laboratory model tunnel test. These bound solutions are also compared with the previous analytical upper and lower bound solutions by Atkinson and Potts (1977) and lower bound solution only by Mühlhaus (1985).

## 2. Review of Bound Solutions in Drained Conditions

Applications of the limit analysis method for the tunnel stability in the drained conditions are shown in Table 1. Each of these applications is well described by Lyamin and Sloan (2000). Among those applications, bound solutions for a shallow tunnel ($C/D \leq 2.5$) by Atkinson and Potts (1977) are particularly considered in this study due to the same soil condition (i.e. $c' = 0$) and independence of the tunnel depth parameter ($C/D$) as well as the magnitude of any ground surface pressure ($\sigma_s$). Atkinson and Potts (1977) derived a lower bound solution (or safe tunnel pressure) based on the possible states of stress in the soil around a shallow tunnel and a upper bound solution (or unsafe tunnel pressure) based on the collapse mechanism, as shown in Figs. 2 (a) and (b) respectively. The lower bound equation is given by

Table 1. Summary of Limit Analysis for the Tunnel Stability problem in Drained Conditions

| References | Limit analysis | Soil conditions | Tunnel geometry | Tunnel depths (C/D) |
|---|---|---|---|---|
| Atkinson and Cairncross (1973) | Lower bound solution | $c'-\phi'$ (Mohr–Coulomb) material | Circular plane strain tunnel | $C/D \leq 2.5$ |
| Atkinson and Potts (1977) | Upper and lower bound solutions | $\phi'$ material ($c' = 0$) | Circular plane strain tunnel | $C/D \leq 2.5$ |
| Mühlhaus (1985) | Lower bound solutions | $c'-\phi'$ (Mohr–Coulomb) material | Circular plane strain tunnel and 3D unsupported cylindrical tunnel heading | $C/D \leq 3.5$ |
| Leca and Dormieux (1990) | Upper and lower bound solutions | $c'-\phi'$ (Mohr–Coulomb) material | Longitudinal unsupported tunnel heading | $C/D \leq 2$ |
| Lyamin and Sloan (2000) | Finite element upper and lower bound solutions | $c'-\phi'$ (Mohr–Coulomb) material | Circular plane strain tunnel | $C/D \leq 5$ |

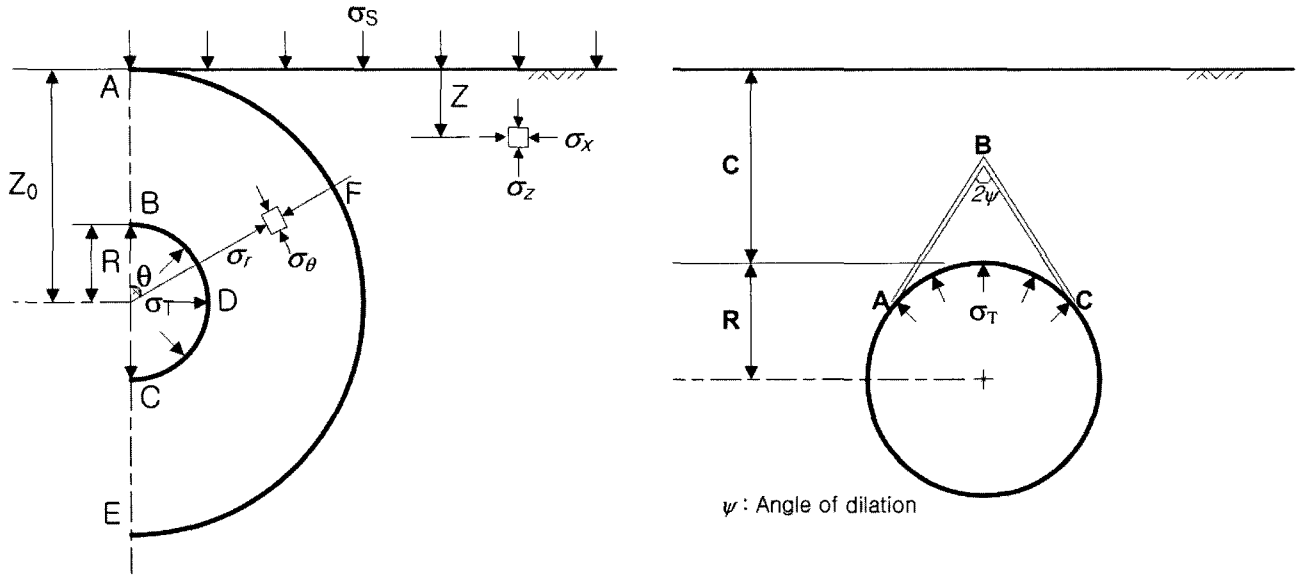


(a) lower bound stress field (b) upper bound mechanism

Fig. 2. Bound solutions after Atkinson and Potts, 1977 ($R$ = tunnel radius, $Z_0$ = depth to tunnel, $\sigma_r$: radial stress around tunnel, $\sigma_\theta$: tangential stress around tunnel)

$$\frac{\sigma_T}{2\gamma R} = \frac{\mu}{(\mu^2 - 1)} \quad (1)$$

where $\mu = \frac{1+\sin\phi'}{1-\sin\phi'}$ and $\phi'$ are the maximum angle of shearing resistance. The upper bound equation is also given by

$$\frac{\sigma_T}{2\gamma R} = \frac{1}{4\cos\phi'}\left(\frac{1}{\tan\phi'} + \phi' - \frac{\pi}{2}\right) \quad (2)$$

It should be noted that the rate of work dissipated in a perfectly plastic frictional material with an associated flow rule ($\psi = \phi'$) is zero and the upper bound, or unsafe, collapse pressure given by Eq. (2) is independent of the tunnel depth ($C$ or $Z_0$) and the magnitude of any ground surface pressure ($\sigma_s$). For a cohesive-frictional ($c'$ - $\phi'$ Mohr-Coulomb) material, Mühlhaus (1985) derived analytical lower bound solutions for a circular plane strain tunnel as well as the three-dimensional problem of an unsupported cylindrical tunnel heading. These solutions are valid for both drained and undrained loading conditions and will be compared with the author's lower bound solution in a later section of this paper.

Recently, Leca and Dormieux (1990) have adopted the limit analysis to provide failure pressures of a shallow unsupported circular tunnel heading in a cohesive-frictional material. They compared their analysis with centrifuge tests and concluded that the upper bound solutions (based on the conical blocks and kinematic conditions) are closer to the actual pressures at failure than the lower bound values, and can assess reasonable estimates of critical face pressures. However, there is a difficulty in deriving precise bounds by hand in three-dimensions (Lyamin and Sloan, 2000). Lyamin and Sloan (2000) have performed the upper and lower bound finite element solutions based on nonlinear programming to assess the stability of a plane strain circular tunnel in a cohesive-frictional material. They showed the deformation patterns and plastic zones for a deep tunnel ($C/D = 5$), which are similar to the authors' FE and the physical model tunnel test data, and also proposed an upper bound rigid block mechanism based on the velocity field at collapse for a material whose friction angle is greater than about 40°. This mechanism is identical to Atkinson and Potts (1977) for the shallow tunnel ($C/D \leq 2.5$).

Apart from the upper bound mechanisms proposed by Atkinson and Potts (1977); Lyamin and Sloan (2000) present the kinematically admissible upper bound mechanisms associated with the maximum shear strain pattern at collapse, which is based on the FEA rather than model

Table 2. Assumed Material Parameters (based on Gibson's soil) for FEA

| c′ (kPa) | ν | $\phi'$ (°) | ψ (°) | $E_0$ (kPa) | $m_E$ (kPa/m) | $m_c$ (kPa/m) | $\gamma'$ (kN/m$^3$) |
|---|---|---|---|---|---|---|---|
| 0.1 | 0.35 | 23 | 15 | 1,600 | 10,000 | 0 | 24 |

Note: $c'$ = cohesion, ν = Poisson's ratio, $\phi'$ = angle of shearing resistance, $\psi$ = angle of dilation, $E_0$ = Young's modulus at ground surface, $m_E$, $m_c$ = gradients of Young's modulus and cohesion with depth, $\gamma'$ = soil unit weight

tunnel test.

## 3. Finite Element Analysis of Model Tunnel Test under Plane-Strain Conditions

Since finite element analysis (FEA) can provide information on all design requirements, the author adopted this method to solve the plane-strain tunnel boundary value problem. The soil behaviour is assumed to be governed by an elastic and perfectly plastic constitutive relation based on the Mohr-Coulomb criterion with a non-associated flow rule, which is incorporated in the CRISP. More details about boundary conditions and tunnelling simulation etc. were explained in Lee (2004). Table 2 summarizes the material parameters derived from the early FE parametric study for pile loading test rather than later shear box test. For this reason, the friction angle ($\phi' = 23°$) and soil unit weight ($\gamma' = 24$ kN/m$^3$) were different from the proposed closed-analytical solution parameters based on the shear box test ($\phi' = 26°$ and $\gamma' = 20$ kN/m$^3$). In the FE work, $K_0$ (= 0.66) was applied to the initial in-situ stress conditions.

### 3.1 Investigation of Stress Paths around FE Tunnel

The model tunnel test was carried out on a truly two-dimensional granular material with no elastic or plastic strains in the transverse direction. $K_f$ line defined as the ultimate critical state is reached at $t/s' = sin\phi'_{cs} = tan\alpha'$ where $s'$ = mean effective stress [= $(\sigma'_1 + \sigma'_3)/2$], $t$ = radius of Mohr's circle of stress [= $(\sigma'_1 - \sigma'_3)/2$]. This line is inclined at angle $\alpha'$ to the normal effective stress axis. The relationship between $t$ and $s'$ of individual elements during the loading or unloading process provides an interesting insight into the local soil behavior. A second important $t/s'$ ratio is the start condition which, in this case, was always an earth pressure at rest ($K_0$ condition). This is termed the $K_L$ line:

$$K_L = \tan\phi'_{k_0} = \frac{t_0}{s'_0} = \frac{(1-K_0)}{(1+K_0)} \quad (3)$$

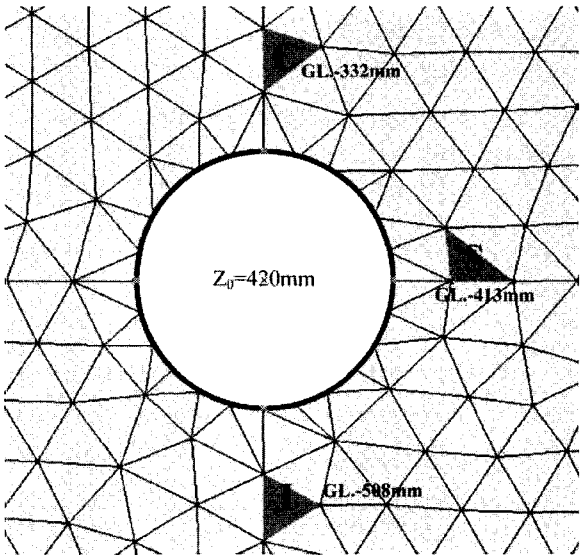


Fig. 3. Locations of soil elements C, S and I around FE tunnel ($Z_0$ = 420 mm)

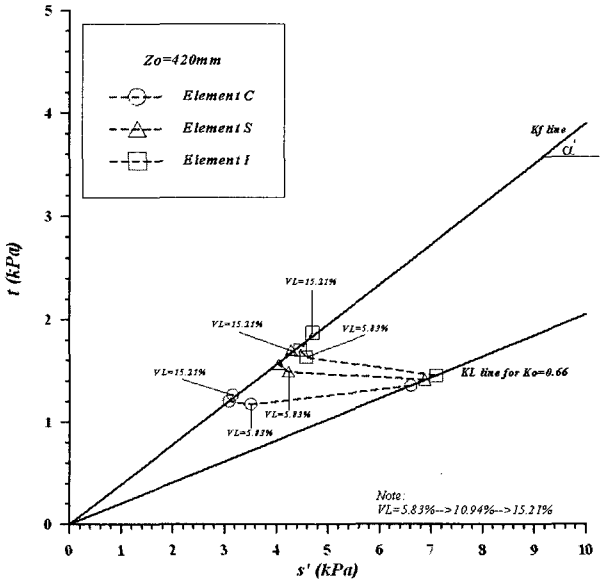


Fig. 4. Stress paths around FE tunnel

where $\phi'_{K0}$ = angle of shearing resistance in $K_0$ condition, $K_0 = (1 - \sin\phi') = 0.66$, the value of $K_L = 0.20$.

Locations of three typical soil elements are shown in Fig. 3. Element C represents soil above the tunnel crown, S to the side of the tunnel (springing) and I below the tunnel (invert) respectively. Fig. 4 shows stress paths for C, S and I soil elements during volume loss developed. The mean normal stress for all elements falls sharply towards the $K_f$ line up to a volume loss of 10.94%, while a marginal increase in shear stress occurs in elements S and I and a small decrease in shear stress occurs at the crown. After 10.94% volume loss, all elements climb slightly along the $K_f$ line. The stress paths are clearly consistent with the tunnel operations (i.e. reducing tunnel diameter), probably reaching a plastic failure condition between 5.83% and 10.94% volume loss.

### 3.2 Investigation of Strain Data

Assuming the numerical work that directions of major principal stress ($\sigma'_1$) and major principal strain ($\varepsilon_1$) coincide for plastic behavior, data from numerical work

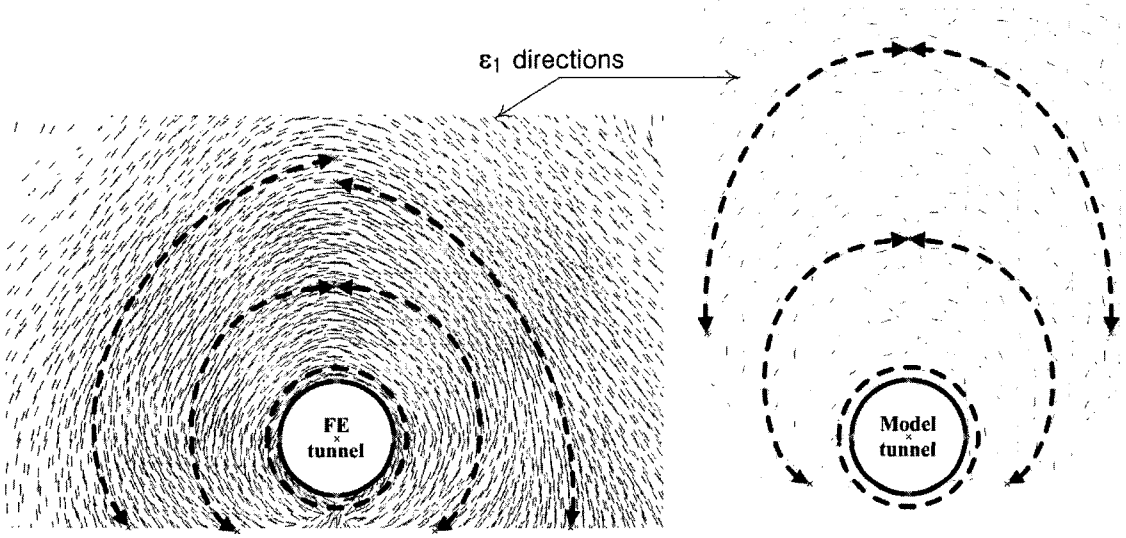


(a) FE tunnel (b) model tunnel

Fig. 5. Comparison of $\varepsilon_1$ (= $\sigma'_1$) directions at $V_L$ = 15.21%

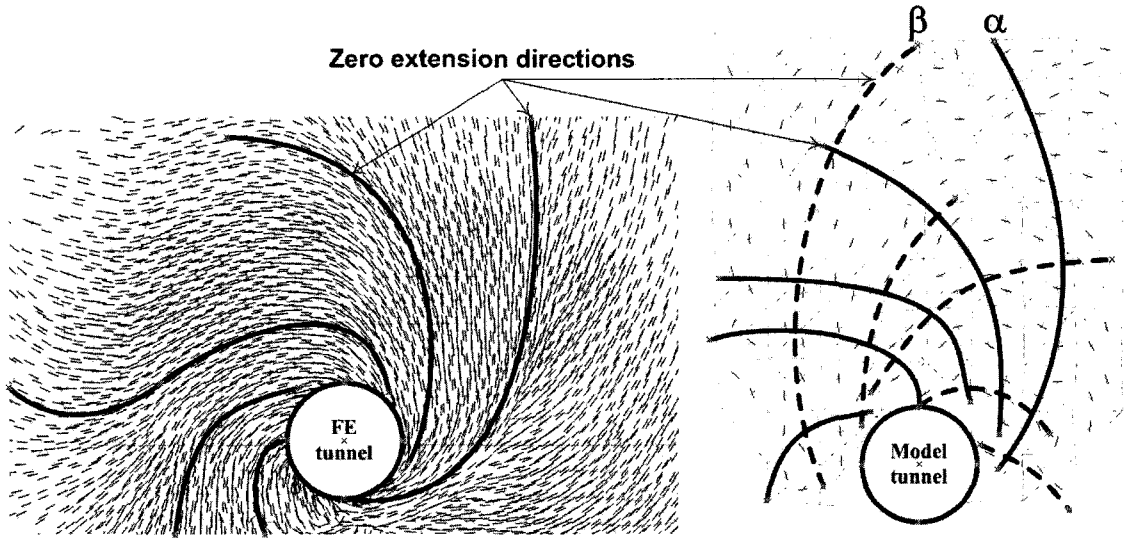


(a) FE tunnel (b) model tunnel

Fig. 6. Comparison of zero extension (slip line) directions at $V_L$ = 15.21%:

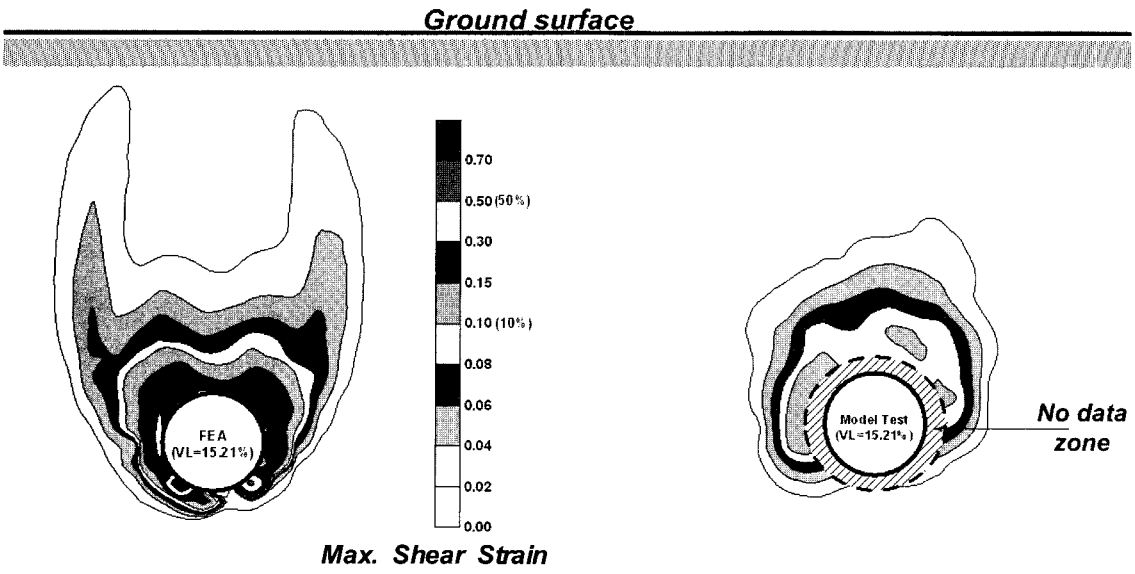


(a) FEA (b) model test

Fig. 7. Comparison of maximum shear strain contour at $V_L$ = *15.21%*

can be compared with the strain data from the physical model tunnel test. $\varepsilon_1$ (= $\sigma'_1$) and zero extensions or slip lines $\alpha$ (positive) and $\beta$ (negative) direction data (based on the Mohr's circle of strain) developed at $V_L = 15.21\%$ are shown in Figs. 5 and 6 respectively. It should be noted that zero extension data from the FEA only present a slip line directions due to the limitation of CRISP program. Surprisingly the pattern of FE data shows fair agreement with the model data. In particular, the tangential orientation of $\varepsilon_1$ (= $\sigma'_1$) directions around the tunnel is identical to model tunnel tests by Atkinson et al. (1977). The author has sketched on the model data some of the best fit trajectories to highlight the similarities. Strain data is notoriously difficult to obtain from small measured differences in physical models. Only the shear strain data is presented in the form of contour plots (Fig. 7). In general, the data from the model suggests the beginning of "horn like" patterns with contours of maximum shear strain, comparable in magnitude and shape, but nothing like which is as dramatic as the FE data.

## 4. Upper and Lower Bound Solutions

The basic concepts for carrying out upper and lower bound approaches are contained in many undergraduate and postgraduate texts. They are well presented by Atkinson (1981). In this study, the author uses the deformation patterns, the shear strain contours and the principal strain (or stress) directions from the physical model test and FE data to assist in their choice of stress fields for lower bound solution and for possible kinematically admissible mechanisms with which to develop the upper bound solutions. In order to be able to draw acceptable stress fields based on straight lines rather than the logarithmic spiral, the author chooses the stress characteristic lines (based on the slip line directions $\alpha$ and $\beta$) that are associated with a $\delta_\theta$ (angle change of $\sigma'_1$ direction) of 15° and a $\phi'$ of 26°. These are able to provide simple whole angles when using $\delta_\theta/2$ and $\rho'/2$. The mobilized friction angle ($\rho'$) and the angles of $\sigma'_1$ direction ($\theta_A$ and $\theta_B$) are calculated, giving the values of $\rho'$, $\theta_A$ and $\theta_B$ and the stress ratio change ($s'_B/s'_A$):

$$\sin\rho' = \sin\phi' \cos\delta_\theta \tag{4}$$

$$\theta_{B\,\&\,A} = (45° + \frac{\rho'}{2}) \pm \frac{\delta_\theta}{2} \tag{5}$$

$$\frac{s'_B}{s'_A} = \exp^{2\Delta\theta \tan\phi'} \tag{6}$$

where $s'_B$ = high stress zone B, $s'_A$ = low stress zone A, $\delta_\theta$ = rotation of principal stress directions [= $\Delta\theta$], $\theta_A$ = angle of principal stress direction in zone A, $\theta_B$ = angle

Table 3. Fundamental Parameters for the Limit Analysis (based on shear box test)

| $\phi'$ (°) | $\rho'$ (°) | $\theta_A$ (°) | $\theta_B$ (°) | $s'_B/s'_A$ | $\Psi$ (°) | $\gamma'$ (kN/m$^3$) |
|---|---|---|---|---|---|---|
| 26 | 25 | 50 | 65 | 1.3 | 26 | 20 |

of principal stress direction in zone B, $\rho'$ = angle of mobilized friction.

Table 3 shows the fundamental parameters used in the limit analysis for the upper and lower bound solutions. It should be noted that the experimental value of $\gamma'$ (*20 kN/m$^3$*) is less than the FE value (*24 kN/m$^3$*). Because the value of g¢ adopted in the FEA was estimated prior to any experimental work. It was assumed that the "area ratio" of rods was much less than the "void ratio" concept of granular material. The packing was assumed to be dense and on the basis of information from Yamamoto and Kusuda (2001). It was assessed that a value greater than *22 kN/m$^3$* would be appropriate for the numerical work.

Bound calculations are relevant to homogeneous, isotropic materials as plastic failure is developed. Lower bounds are assumed on equilibrium across "stress discontinuities" and the Mohr's circle of stress is used to determine the stress changes. Upper bounds incorporate a complete kinematically admissible rupture mechanism. The best answers are obtained when the collapse mechanisms and the stress discontinuity pattern are common.

## 4.1 Lower Bound (LB) Solution

Fig. 8 shows the two stress discontinuities $\alpha$ and $\beta$ for a material with $\phi' = 26°$ and $\delta_\theta = 15°$. Mohr's circles of stress for typical zones A and B are shown in Fig. 9. The two discontinuity lines $\alpha$ and $\beta$ together with the major principal stress directions are shown. The resulting circumferential arrangement of $\sigma'_1$ directions was as observed in both the model tunnel test and the FEA data.

To assess a lower bound solution for a tunnel at a specific depth ($Z_0 = 420$ *mm*) involves a uniform stress distribution around the whole tunnel and produces the "tear drop" type diagram between the ground surface at m and the tunnel, as shown in Fig. 10. The diagram is for a weightless material with a surcharge at m. Self weight soil would deform this pattern. However, two approximate answers can be obtained as follows: (a) the tear drop is assumed to be bound to the fully mobilized plastic zone; (b) At the level of the centre line of the tunnel point v in the elastic zone, the principal stress direction is vertical and is assumed to be the self weight. Area V is assumed to be at the limiting active state:

$$(\sigma'_3)_v = K_A(\sigma'_1)_v \tag{7}$$

where $K_A = \dfrac{(1-\sin\phi')}{(1+\sin\phi')}$ and $\sigma'_1$, $\sigma'_3$ = major and minor principal effective stresses, therefore

$$s'_v = \frac{(\sigma'_3)_v}{(1-\sin\phi')} = \frac{K_A(\sigma'_1)_v}{(1-\sin\phi')} = \frac{(\sigma'_1)_v}{(1+\sin\phi')} \tag{8}$$

Between zone V and zone R adjacent to the tunnel there are 8 stress discontinuities finishing at the same physical level. Therefore, the value of $P_0$ (= $\sigma_T$) at the tunnel centre level will be

$$(\sigma'_3)_R = \frac{K_A(\sigma'_1)_v}{(1.3)^8} \tag{9}$$

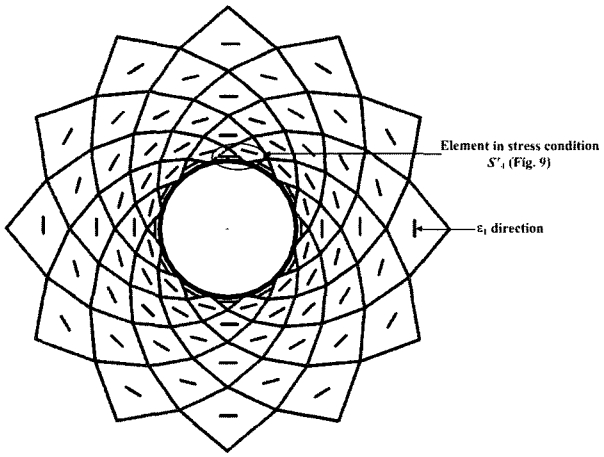


Fig. 8. Postulated stress discontinuities associated with $\phi'$ = 26° and $\delta_\theta$ = 15°

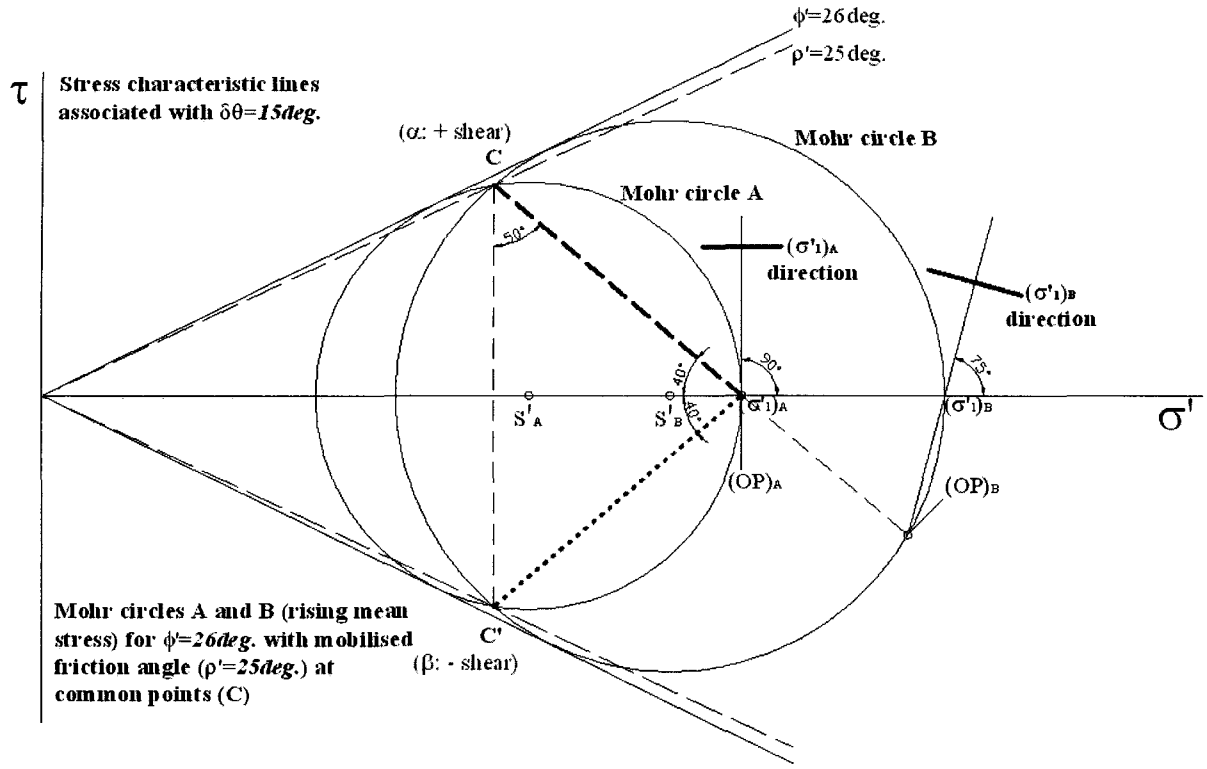


Fig. 9. Mohr circles with $\alpha$ and $\beta$ discontinuities for zone A

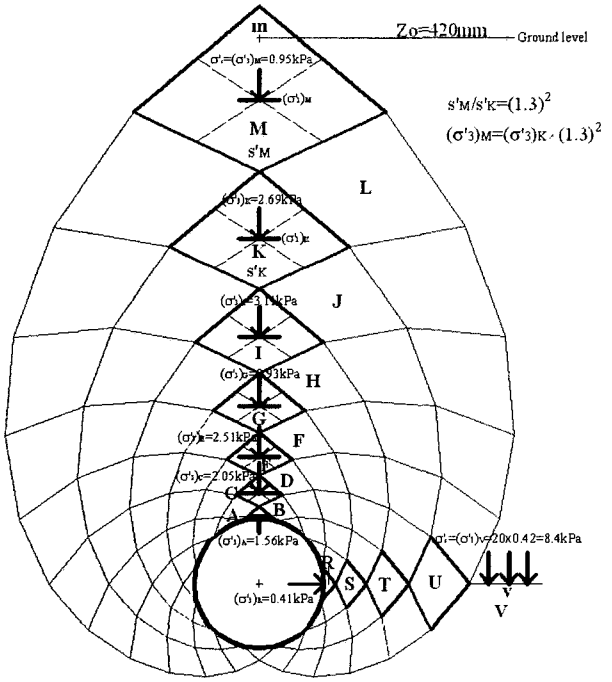


Fig. 10. Lower bound stress field for $Z_0 = 420\ mm$ tunnel

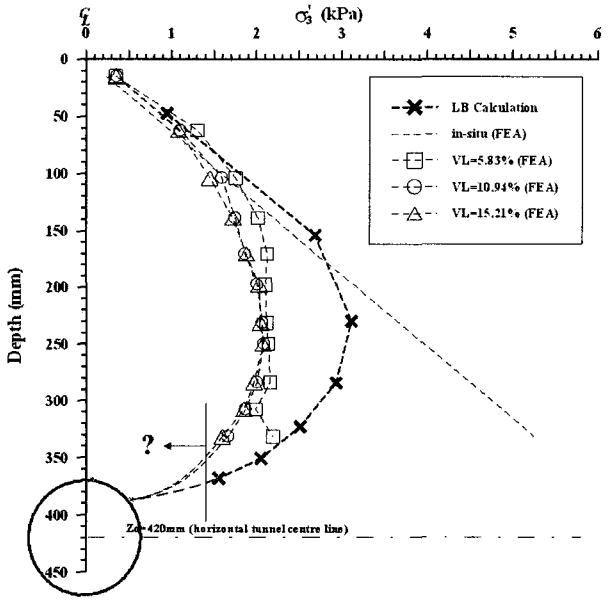


Fig. 11. Comparison of $\sigma'_3$ above tunnel crown (along tunnel centre line)

A similar exercise has been carried out down the vertical axis from M to A by a simple "two step method" adjusting the $s'$ value for each double step. This yielded a value of *1.56 kPa* (= $(\sigma'_3)_A$). It is believed that the horizontal assessment is the more relevant value as the distorted form of stress discontinuities would be less influential across the horizontal axis. Also, the failing zones developed in this area rather than at the crown.

As an interesting check, the author investigates the $\sigma'_3$ stress distribution down the vertical centre line of the tunnel with the FE data, as shown in Fig. 11. The pattern

of stress distribution from the LB calculation is in agreement with the FE data for large volume losses $V_L$ = *10.94%* and *15.21%*, but clearly diverges to some 1.1 kPa higher below 150 mm. The FEA could not provide data below 330 mm due to the influence of the bar elements but a value of about 0.7 to 0.8 kPa would appear to be probable. A similar discrepancy and stress distribution down the tunnel axis are observed between the LB calculation for 230 mm depth and 250 mm for the FEA.

## 4.2 Upper Bound (UB) Approach

Based on the "tear drop" stress discontinuity field adopted for the lower bound, the author examined many possible

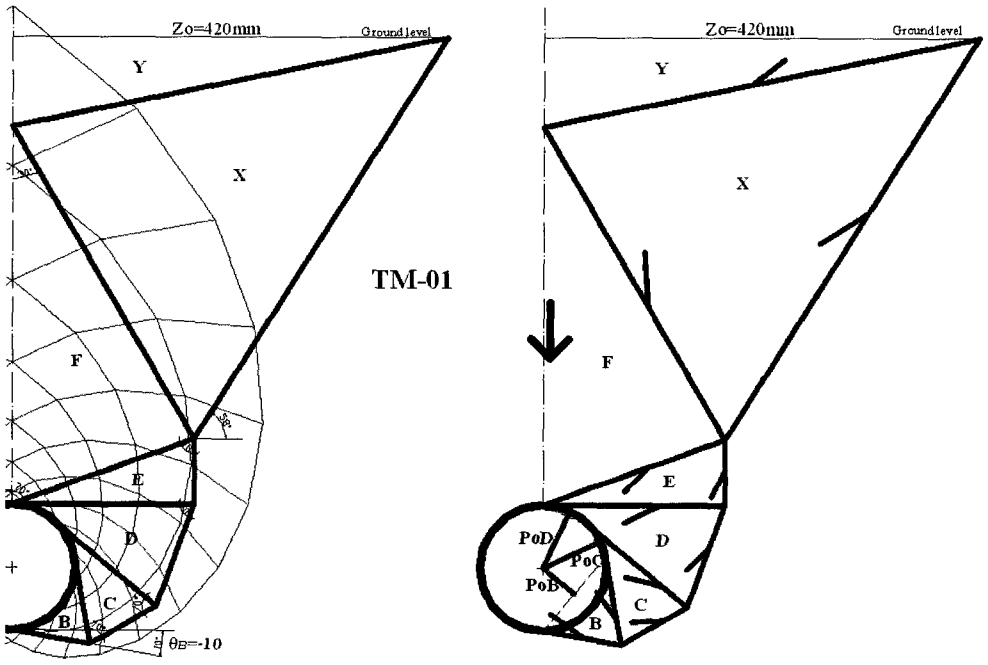


Fig. 12. Upper bound mechanism, TM-01

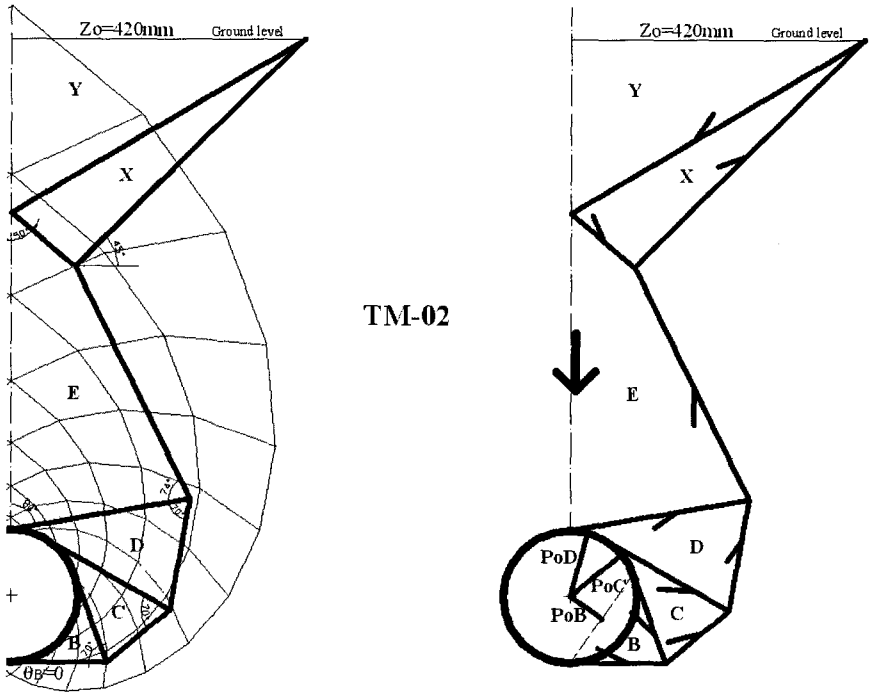


Fig. 13. Upper bound mechanism, TM-02

mechanisms. Three of the possible kinematically admissible failure mechanisms (viz. TM-01; TM-02; and TM-03) are shown in Figs. 12, 13 and 14. The key differences are the orientation of the initial block B (i.e. 10° below horizontal; horizontal; and 23° above horizontal) and the active subsidiary blocks X and Y which enter the "elastic zone". The displacement vectors on rupture surfaces are shown as a short solid line. The corresponding displacement diagrams for these upper bound mechanisms are shown in Fig. 15. The radial movements of the segments adjacent to the tunnel are assessed and a uniform pressure $P_0$ (or $\sigma_T$) is assumed to act radially over the whole tunnel surface. The work done against the $P_0$ stress is equated to the self weight work contribution (based on full association, $\phi' = \psi$, no work is dissipated within the soil).

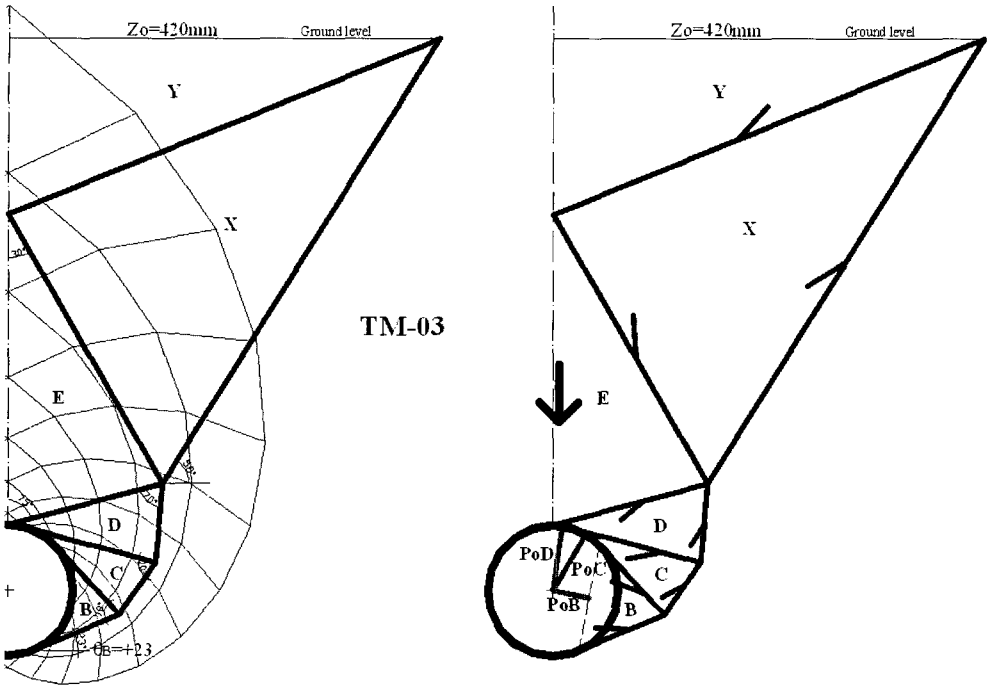


Fig. 14. Upper bound mechanism, TM-03

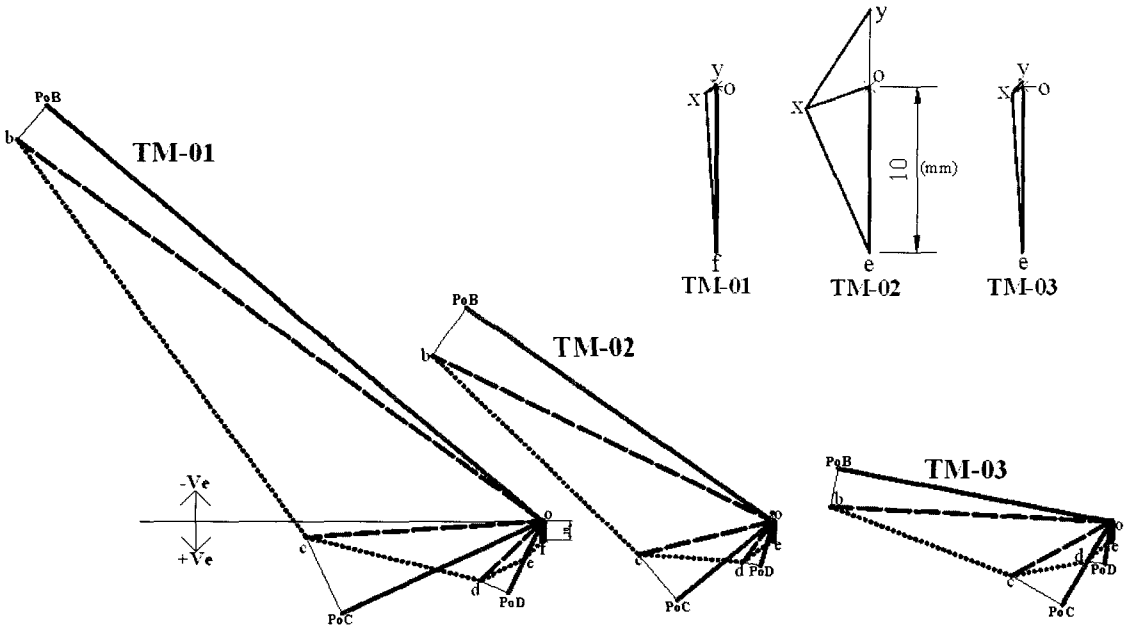


Fig. 15. Corresponding displacement diagrams for TM-01, 02 and 03

## 5. Results

The values of $P_0$ from the lower and upper bound solutions are summarized in Table 4. The upper bound solutions for mechanisms TM-01 and TM-02 are surprisingly close to the lower bound solution for the tunnel centre line level. It is believed this was achieved because of the large radial movements resulting from the displacement of segment B dominating the work component. This segment incorporates the zone at and below the tunnel centre line.

Fig. 16 shows the location of FE elements C*, P*, R* and S* around the FE tunnel. In Fig. 17 the minor principal stress ($\sigma'_3$) for each FE element is plotted against volume loss ($V_L$). For comparison, the lower bound solutions in two crown locations are also shown. The stresses all appear to decay towards an asymptotic value as volume loss increases, stabilizing at between 1.45 and 1.65 kPa. It should be noted that the elements chosen are not right against the tunnel surface, but somewhat inside this line. This was because the presence of the "bar elements" in the FEA caused major fluctuations in the $\sigma'_3$ values at the various integration points in the crown elements close to the tunnel surface. The lower bound solution for A is in surprisingly good agreement with the FE data for the crown elements C* (on the centre line) and P* (on the 45° line). In addition, the lower bound solution by Mühlhaus (1985) is close to the LB at A, while an analytical LB solution by Atkinson and Potts (1977) is remote from those LB solutions. The remote LB value is probably due to their assumption of admissible stress boundary conditions – if the critical location is at tunnel crown B in Fig. 2 (a) for $Z_0 = R = D/2$ (i.e. tunnel crown level is located at ground surface, $C = 0$), the tunnel pressure ($\sigma_T$) can become a major principal stress ($\sigma'_1$) rather than a minor principal stress ($\sigma'_3$) in this study, i.e. $\sigma_{rB} = \sigma'_1 = \sigma_T$ and $\sigma_{\theta B} = \sigma'_3 = \sigma_T/\mu$. For this reason, their LB solution is

Table 4. $P_0$ Values from LB and UB Approaches

| LB | | | | UB | | |
|---|---|---|---|---|---|---|
| Crown area | | Centre level | | | | |
| C | A | S | R | TM-01 | TM-02 | TM-03 |
| 2.05kPa | 1.56kPa | 0.7kPa | 0.41kPa | 0.48kPa | 0.50kPa | 6.31kPa |

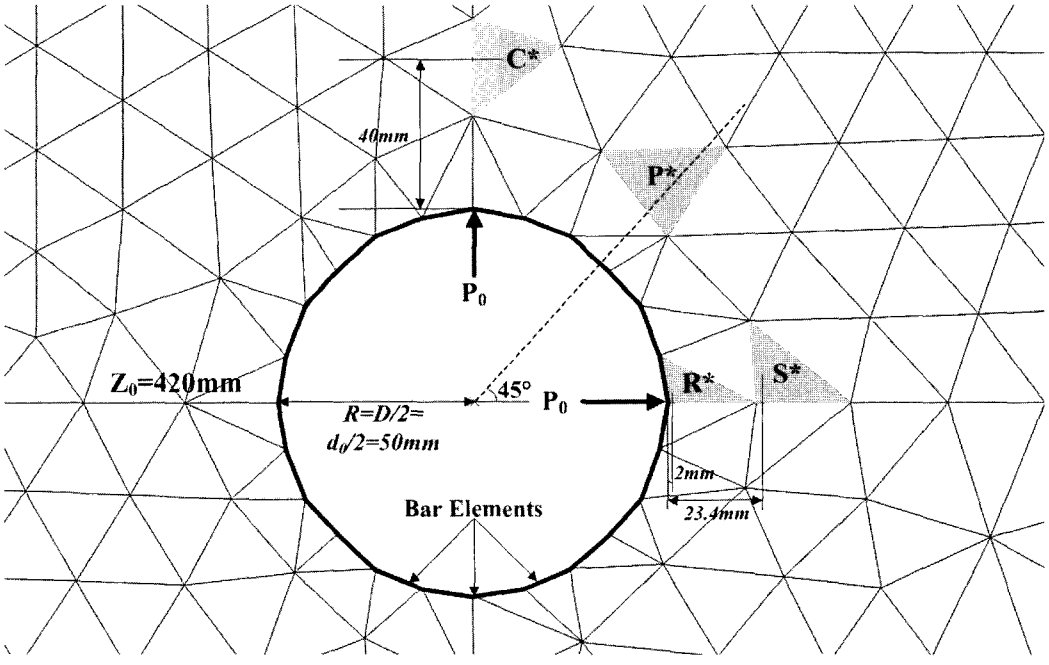


Fig. 16. Soil elements C*, P*, R* and S* around FE tunnel

more appropriate for shallow tunnels rather than deep tunnels ($C/D > 2.5$). However, the LB solution by Atkinson and Potts (1977) indicates critical tunnel pressure in terms of safety, i.e. safe tunnel pressures must lie on or above the LB solution.

Fig. 18 shows the two lower bound values for the horizontal locations R and S and the UB value for TM-01 together with the FE data for R* and S*. In contrast to the FE soil elements adjacent to the tunnel crown surface, the FE element R* (on the horizontal tunnel axis) appears to be very close to the lower bound solution for the location of R. The FE element S* shows a rapid stress degradation as volume loss develops, approaching an asymptotic value close to the lower bound solution for the location of S. Surprisingly the UB value from Atkinson and Potts (1977) for $\phi' = 26°$ is very close to the author's result for TM-01. Their kinematically admissible upper bound mechanism shown in Fig. 2 (b) seems to work for the deep tunnel. However, it is obvious that Atkinson and Potts's (1977) LB and UB solutions for the tunnel pressure are mainly dependent of soil strength parameter ($\phi'$) and unit weight of soil ($\gamma'$) rather than tunnel geometry parameter ($C/D$). Therefore, their bound solutions could strictly be limited to the shallow tunnels. Nonetheless, for a high frictional material ($\phi' = 50°$), the LB solution by Atkinson and Potts (1977) is in good agreement with Mühlhaus (1985) considering the tunnel geometry parameter ($C/D$) additionally in his LB solution (Fig. 19). From the above point of view, the soil strength parameter ($f\phi$) particularly around the tunnel plays a key role in the deep tunnel pressure for Atkinson and Potts (1977).

The author believes that the stresses in the FE elements chosen adjacent to the tunnel side wall are much less influenced by the "bar elements" than those on the crown. The tunnel sides are almost a classic "active retaining wall" situation.

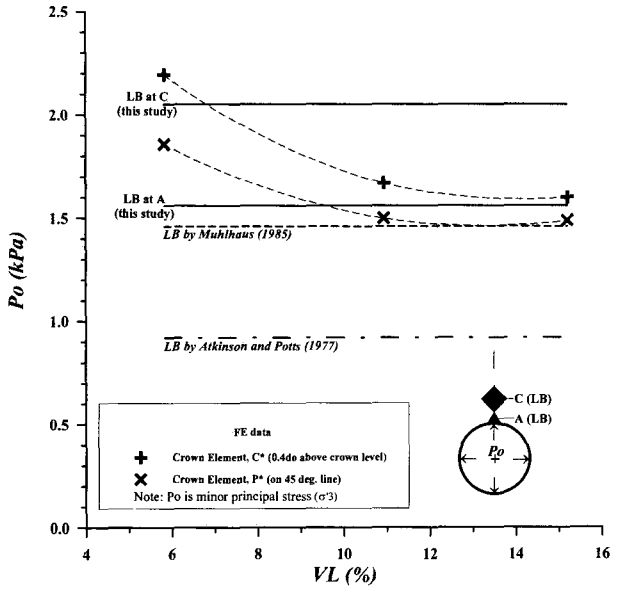


Fig. 17. LB solutions for A and C with FE data ($\sigma_s = 0$, $\phi' = 26°$)

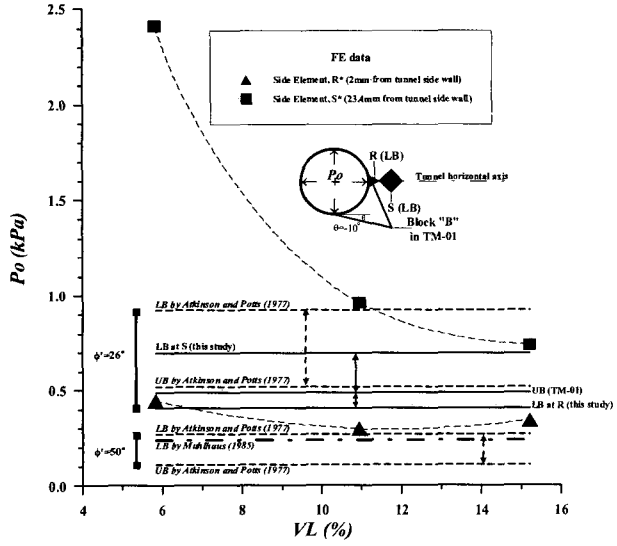


Fig. 18. UB solution for TM-01 and LB solutions for R and S with FE data

## 6. Conclusions

Failure mechanisms (based on the "tear-drop" stress discontinuity field) of a relatively deep circular plane-strain tunnel in a cohesionless-frictional material have been proposed using the finite element analysis (FEA) and the physical model tunnel test. The tunnel collapse pressures assessed by the upper and lower bound approaches in this paper were shown to be in good agreement with the FE results, in particular the FE soil elements located on the horizontal tunnel axis. However, the lower bound assessment proved quite difficult between the ground surface and the tunnel crown (i.e. along the vertical axis of the tunnel), where the soil self-weight influence was only approximately allowed for.

## References


1. Atkinson, J. H. (1981), "Foundations and slopes", McGraw-Hill, UK.
2. Atkinson, J. H. and Cairncross, A. M. (1973), "Collapse of a shallow tunnel in a Mohr-Coulomb material", *Proc. Symp. Role of plasticity in soil mechanics*, Cambridge, 202-206.
3. Atkinson, J. H. and Potts, D. M. (1977), "Stability of a shallow circular tunnel in cohesionless soil", *Géotechnique*, 27, 203-215.
4. Atkinson, J. H., Brown, E. T., and Potts, D. M. (1977), "Ground movements near shallow model tunnels in sand", *Proc. Conf. of Large ground movements and structures*, J. D. Geddes (ed.), The University of Wales Institute of Science and Technology, Cardiff, July 1977, 372-386.
5. Leca, E., and Dormieux, L. (1990), "Upper and lower bound solutions for the face stability of shallow circular tunnels in frictional material", *Géotechnique*, 40, 581-606.
6. Mair, R. J., and Taylor, R. N. (1997), "Theme lecture: Bored tunneling in the urban environment", *Proc., 14th Int. Conf. Soil Mech. Found. Engrg.*, Vol.4, 2353-2385.
7. Mühlhaus, H.-B. (1985), "Lower bound solutions for tunnels in two and three dimensions", *Rock Mech. Rock Eng.*, 18, 37-52.
8. Lee, Y. J. (2004), "Tunnelling adjacent to a row of loaded piles", PhD thesis, University College London, University of London, UK.
9. Lyamin, A. V. and Sloan, S. W. (2000), "Stability of a plane circular tunnel in a cohesive-frictional soil", *Developments in theoretical geomechanics: Proc., of the Booker memorial symposium*, J. P. Carter and D. W. Smith (eds.), Balkema, Rotterdam, 139-153.
10. Yamamoto, K. and Kusuda, K. (2001), "Failure mechanisms and bearing capacities of reinforced foundations", *Geotextiles and Geomembranes*, 19, 127-162.


(접수일자 2007. 3. 20, 심사완료일 2007. 5. 2)